STM JOURNALS

Journal of
Polymer & Composites

https://journals.stmjournals.com/jopc

ISSN: 2321-2810 (Online)
ISSN: 2321-8525 (Print)
Volume 14, Issue 2, 2026
DOI (Journal): 10.37591/JoPC

Research JoPC

AI-Driven Topology Optimization of Woven Fiber-Reinforced Composite Chassis Structures for Electric Vehicles Under Crash Loading

Sweety Jachak[1], Pankaj Vispute[2], Sapna Sonar[3], Swapnil Ratnakar[4], Piyush Bhamare[5], Gokul Mahajan[6], Krupal Pawar[7,*]

Abstract

The structural design of an electric vehicle (EV) chassis represents a unique engineering challenge to achieve minimal weight while meeting occupants' safety requirements during high-energy crash conditions without compromise to the battery housing's integrity or the geometrical constraints of the electric powertrain package. In this paper, a single framework is proposed to integrate physics-based artificial intelligence (AI) surrogate models using PINNs, CNN-accelerated topology optimization, and FEA to design woven fiber-reinforced polymer (WFRP) composite chassis components that are optimized specifically for frontal, side, and rear crash loading conditions. Due to the complex interlocking geometry of the woven reinforcement and the manufacturing anisotropy of the fabric, the complex geometry and the anisotropy of the fabric are directly modeled in the constitutive relationship of the material and the AI surrogate. Starting with a three-dimensional design space discretized into 1.2 million hexahedral elements, the proposed pipeline significantly reduced the optimization wall clock time by 78% relative to the SIMP method while providing a 14.3% reduction in mass and an 11.7% increase in the specific energy absorption (SEA) of the WFRP chassis component relative to a similar mass steel reference structure. A progressive damage model was used to model the inter-fiber crack growth and the matrix crack growth under dynamic crushing of the fiber tow and the matrix. The progressive damage model incorporates the Hashin failure criterion and a modified Puck inter-fiber fracture model. The developed framework was verified by comparing the predicted response to drop tower test data and sled test data from a purpose-built EV prototype chassis, indicating that the prediction error of the peak crush force was less than 7.2%, and the prediction error of the SEA was less than 5.9%. These results indicate that AI-based composite topology optimization is ready to be deployed in industry as a tool for designing EV chassis components.

***Author for Correspondence**
Krupal Pawar
E-mail: krupalpawar@gmail.com

[1]Assistant Professor, Department of Computer Engineering, Guru Gobind Singh College of Engineering and Research Centre, SPPU, Nashik, Maharashtra, India
[2]Assistant Professor, Department of Electronics and Telecommunication Engineering, Shatabdi Institute of Engineering and Research, SPPU, Nashik, Maharashtra, India
[3]Assistant Professor, Department of Electrical Engineering, Shatabdi Institute of Engineering and Research, SPPU, Nashik, Maharashtra, India
[4-6]Assistant Professor, Department of Mechanical Engineering, Shatabdi Institute of Engineering and Research, Nashik, Maharashtra, India
[7]Assistant Professor, Department of Mechanical Engineering, Rajiv Gandhi College of Engineering, SPPU, Ahilyanagar, Maharashtra, India

Received Date: March 05, 2026
Accepted Date: March 16, 2026
Published Date: April 01, 2026

Citation: Sweety Jachak, Pankaj Vispute, Sapna Sonar, Swapnil Ratnakar, Piyush Bhamare, Gokul Mahajan and Krupal Pawar. AI-Driven Topology Optimization of Woven Fiber-Reinforced Composite Chassis Structures for Electric Vehicles Under Crash Loading. Journal of Polymer & Composites. 2026; 14(2): 72–89p.

Keywords: Structural design, electric vehicle, PINNs, CNN-accelerated topology optimization, WFRP

INTRODUCTION

The shift in global vehicle production towards electric vehicles has led to a transformation of all areas of automotive engineering. As opposed to IC engines which do not contain a high-energy-density component in addition to being less expensive and less structurally sensitive, electric vehicles are equipped with battery packs that provide both the highest energy density and expense as well as structural sensitivity as any other component

onboard. Therefore, a chassis that is unable to protect its battery pack in the event of a crash does not only expose the vehicle to catastrophic fire risk; however, it also eliminates any potential regulatory pathway to market for the vehicle. This establishes a design paradigm that is fundamentally different than traditional structural analysis of passenger cars: the chassis must be light enough to support maximum vehicle range while maintaining sufficient structural rigidity to ensure acceptable noise vibration harshness (NVH) performance while being sufficiently crashworthy to meet the entire matrix of Federal Motor Vehicle Safety Standards (FMVSS), National Highway Traffic Safety Administration (NHTSA) New Car Assessment Program (NCAP) and United Nations Economic Commission for Europe (UNECE) Global Technical Regulations (UN-GTR) crash standards [1].

A number of studies have identified Fiber Reinforced Polymer (FRP) composites as candidate materials for structural components in Electric Vehicles due to their superior specific stiffness and specific strength compared to traditional metallic structures [43]. Structures made using carbon-fiber reinforced polymers (CFRP) produced through autoclave curing have exhibited specific energy absorption values greater than 120 J/g in axial crush testing, far exceeding the 20–40 J/g range observed in thin-walled steel sections [2]. However, the cost and cycle time penalties associated with producing CFRP structures through prepreg-autoclave processing have driven increasing interest in woven architectures that can be produced using liquid composite molding (LCM) processes including resin transfer molding (RTM) and vacuum-assisted resin infusion (VARI). Woven composites exhibit improved in-plane isotropy, increased out-of-plane interlaminar shear strength, and improved drape characteristics over complex tool geometries compared to unidirectional prepregs. Additionally, woven composites have more favorable recycling characteristics than unidirectional prepregs [3, 4].

Topology optimization (TO) offers a theoretically sound methodology for redistributing material within a given design domain in order to minimize compliance and/or maximize energy absorption subject to volume and manufacturing constraints. Density-based methodologies such as SIMP [5] and BESO [6] have been modified to include fiber angle optimization [7] and free material optimization [8] for composite laminates. While classical TO methods are computationally intensive, particularly when applied to high resolution three dimensional models subjected to nonlinear dynamic loads (a single crash simulation for an automotive substructure may take 6–48 hours of CPU time on a large parallel cluster, and thousands of simulations will be performed during the optimization process [9]), machine learning and deep learning techniques have been proposed as efficient surrogate and acceleration tools for structural optimization workflows. Specifically, convolutional neural networks have shown the capability to learn the relationship between the boundary conditions and load cases and the optimal topology distribution with inference times on the order of milliseconds instead of hours [10, 11]. Additionally, physics-informed neural networks incorporate governing equations into the loss function to reduce the need for labeled data and improve the generalization of the network outside of the training distribution [12]. Graph Neural Networks (GNNs) represent a mesh invariant formulation suitable for unstructured finite element meshes [13].

The application of these developments to isotropic metallic structures and simple composite laminates has been reported; however, the development of an application to woven FRP composites subjected to crash loading where material nonlinearity, progressive damage and contact mechanics interact simultaneously is a significant open research problem. This paper presents a tightly integrated workflow described in detail in the subsequent sections to address this open research challenge. In Section 2, relevant prior work is surveyed and the specific gaps filled by this research are identified. In Section 3, the material constitutive model for plain weave CFRP and GFRP is developed. In Section 4, the AI-driven topology optimization framework is presented. In Section 5, the finite element crash model and the progressive damage formulation are detailed. In Section 6, the experimental validation program is outlined. In Section 7, results are presented and benchmarked. In Section 8, limitations and future directions are discussed. Finally, Section 9 summarizes the conclusion.

LITERATURE REVIEW

Topology Optimization for Composite Structures

In addition to the classical SIMP approach introduced by Sigmund [14] that still dominates commercial codes due to its ease of implementation and guaranteed convergence, other types of approaches have been developed in the past two decades. For example, in [7], composite laminates are treated through the encoding of the lamination parameters as design variables so that both the optimization of the material distribution and the orientation of the fibers can be carried out simultaneously. The DMO (Discrete Material Optimization) method was introduced by Stegmann and Lund [15], in order to parameterize the candidate fiber angles through a weighted sum, thus avoiding the non-convexity of the continuous angular variables. Recently, the FMO (Free Material Optimization) method has been used to determine the locally optimal and un-constrained orthogonal material tensors, that can be then used to reconstruct the manufactural laminate stacking sequences [8].

Topology optimization for crashworthiness is different from classical topology optimization since the objective function, typically SEA or maximum crash force at prescribed displacement, is defined on a nonlinear and history dependent structural behavior. A hybrid cellular automaton (HCA) algorithm for crash TO was proposed by Patel et al. [16], which defines the material density according to the internal energy density distributions obtained through explicit FE analysis. The HCA algorithm has been combined with progressive damage models for composite structures [17]. Equivalent Static Load (ESL) methods [18] represent another way to treat crash loading. These methods transform a dynamic crash load problem into a sequence of static problems allowing the use of gradient-based TO algorithms; however, they introduce approximations that increase as the geometrical and material nonlinearities of the composite structure increase during a crash event. (Figure 1.)

Woven Composites: Mechanical Characterization and Failure

The deformation and failure of Woven Fiber-Reinforced Polymer (FRP) composite laminates can be traced back to its intricate structure of interlacing warp and fill tows and the matrix rich interfaces that exist between them. Meso-scale models that describe the mechanical behavior of woven composites include the binary model of Cox and Flanagan [19] which decomposes the stiffness of each tow into an axial contribution (to bear load) and a transverse contribution (to constraint). These models enable the prediction of elastic constants of the laminate using a combination of volume fraction of fibers and geometry of tow crimp. However, these models require prohibitively expensive computational resources when they are used in conjunction with a Total Optimization (TO) loop. To predict failure of woven composites, it is necessary to employ multi-scale and multi-mechanism failure criteria. The failure criteria of LaRC04 [21], developed by Dávila et al., and those of Puck [22] are generally considered to be the most accurate of the current generation of in-plane failure criteria for woven composites.

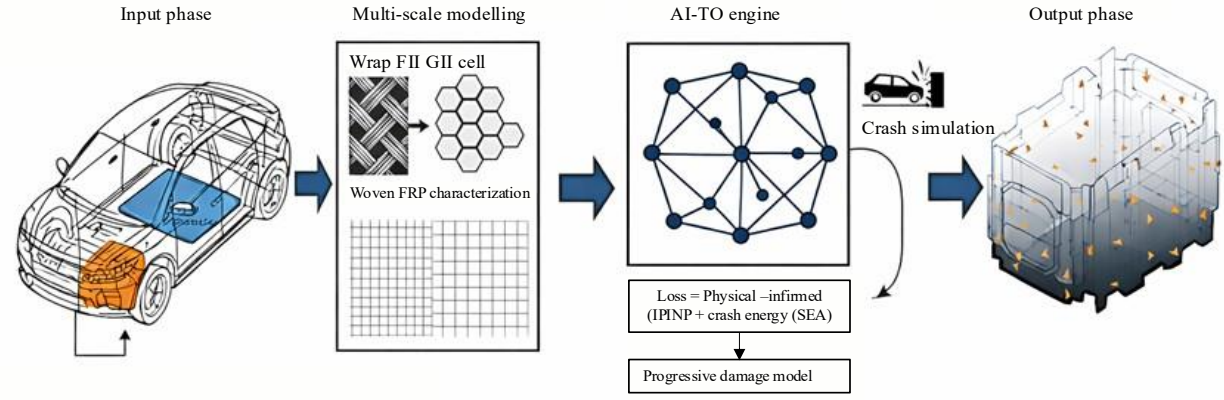

Figure 1. Crashworthiness-specific topology optimization.
*(**Source:** Original image)*

Both criteria capture fiber tensile fracture, fiber compressive micro-buckling, matrix cracking and delamination initiation as separate entities, through analytical expressions. At high strain rates relevant to crashworthiness applications, the tensile strength and failure strain of carbon fiber tows show very little variation with respect to the loading rate, whereas the matrix dominated material properties such as in-plane shear strength and interlaminar shear strength show significant strain rate effects [23]. A number of researchers have proposed and validated rate dependent viscoelastic constitutive models of woven CFRP over a strain rate range of approximately 10^{-3} to 10^{3} s^{-1} [24].

Machine Learning in Structural Optimization

Topology Optimization is a field of study where a designer uses computational methods to optimize structural performance and material usage. While there are many different methods available, they often require high amounts of computation time and can be difficult to interpret. Deep learning has become increasingly popular as researchers use it to help design structures that are lightweight yet strong. Researchers Sosnovik and Oseledets [10] were the first to show that deep learning could be applied to topology optimization and this was shortly after Banga et al. [25] showed that convolutional neural networks (CNNs) could predict two dimensional binary density fields for fixed boundary condition problems. Lin et al. [26] proposed the TopNet Framework which was an encoder-decoder model with skip connections to allow generalization over various loading cases and to allow for fractional design. GANs (Generative Adversarial Networks) [27] were also shown to be useful in creating a large number of candidate designs with varying levels of complexity, and VAEs (Variational Autoencoders) [28] were shown to provide a means of exploring the design space through latent space.

Raissi et al. [12] developed the concept of physics-informed neural networks (PINNs) to solve partial differential equations. PINNs have since been applied to solid mechanic's problems such as plane stress problems in which the equilibrium equations, compatibility conditions and constitutive laws are encoded into the loss function of the neural network. Haghighat et al. [29] demonstrated that PINNs can be applied to plane stress elasticity problems with competitive results compared to finite element analysis but at much lower cost. One of the challenges associated with applying deep learning to composite laminates is encoding the anisotropic constitutive law and the layup dependent coupling terms into the PINN architecture. This problem was solved by Nguyen-Thanh et al. [30] by developing a deep energy method formulation to encode the anisotropic constitutive law. Graph Neural Networks (GNNs) have been used by Pfaff et al. [13] to simulate mesh based physical systems at rates many orders of magnitude greater than traditional solvers. However, their application to progressive damage in woven composites is largely unexplored.

Composite EV Structures: Current State of Practice

The BMW i3/i8 and subsequent European Union (EU) project ALIVE (Multi-Material Topology Optimization for Automotive Platforms), as well as CAE-COMPOSITES (Advanced Composite Materials for Automotive Structures) projects were directed at developing automotive multi-material topological optimized platforms combining Aluminum, Carbon Fiber Reinforced Polymer (CFRP) and Glass Fiber Reinforced Polymer (GFRP) in hybrid composite structures [32]. Frontal crash energy management in composite electric vehicles (EVs) has been thoroughly investigated by Feraboli & Nordenholz [33] who modeled crush front progression in CFRP sine-wave beams. More recent studies include those of Patel & Choi [34] that used woven GFRP composite crash cans with trigger features that provided specific energy absorption (SEA) values of 48–65 J/g based upon lay-up sequence; these composite crash cans also exhibited stable progressive crush modes when compared to NCAP pole-impact protocols (Figure 2).

However, despite the significant body of knowledge regarding the use of woven FRP composites in crash applications, the use of artificial intelligence (AI)-driven topology optimization in conjunction with woven FRP progressive damage modeling for complete EV chassis crash scenarios is largely unexplored.

Figure 2. Woven Fiber-reinforced composite sample.
(Source: Original Image)

Most previous studies have utilized AI-based topology optimization methods that have been validated against linear-static benchmark conditions [35] and/or simplified two-dimensional structures [36]; few studies have addressed the complex packaging constraints associated with the protection of an EV's battery tray from intrusion during all crash modes [37]. Therefore, the current study was specifically developed to address these gaps.

MATERIAL CONSTITUTIVE MODEL FOR WOVEN CFRP

Meso-Scale Architecture and Homogenization

A plain-weave Toray T700SC-12K carbon fiber fabric was selected for this investigation and was consolidated into an Araldite LY1564/HT9075D epoxy resin matrix using the RTM method. This produced a fiber volume fraction of $V_f = 0.55 \pm 0.02$. The fabric had a tow spacing of 3.2 mm, a weave pitch of 3.6 mm and a nominal ply thickness of 0.25 mm. A representative unit cell (RUC) was generated using the TexGen software package; the RUC is based on a simple representation of the fabric's structure, where the centerlines of the yarns were represented by sinusoidal functions of equal amplitude to one-half of the ply thickness. Using periodic boundary conditions, the properties of the representative unit cell were homogenized to produce effective elastic moduli at the laminate level, and these were subsequently converted to engineering constants: $E_{11} = 63.4$ GPa, $E_{22} = 62.8$ GPa (as nearly perfectly balanced) $G_{12} = 4.7$ GPa, $\nu_{12} = 0.04$. The measured values were further validated against those measured during quasi-static coupon testing performed in accordance with ASTM D3039 (tension), ASTM D3518 (shear) and ASTM D6641 (compression). Additionally, through-thickness modulus ($E_{33} = 9.6$ GPa) and interlaminar shear modulus ($G_{23} = 3.8$ GPa) were measured using ultrasonic C-scan velocity measurements, and corrected for by applying the self-consistent micromechanics scheme of Chamis [38], such that they could be utilized as input into both the constitutive module within the PINN and the explicit FEA material card, allowing for consistency of the materials' properties across the different length scales.

Progressive Damage Formulation

The progressive damage model for woven CFRP is developed using a continuum damage mechanics (CDM) approach and three damage variables d_1, d_2 and d_{12} to describe the tensile/compressive failure of warp tows, tensile/compressive failure of fill tows and in-plane shear failure, respectively. Damage initiation occurs when one or both of the Hashin [39] criteria for tensile fiber and matrix damage occur:

Fiber tensile ($\sigma_{11} \geq 0$): $(\sigma_{11} / X\_T)^2 + \alpha(\tau_{12} / S\_L)^2 \geq 1$ (1)

Matrix tensile ($\sigma_{22} \geq 0$): $(\sigma_{22} / Y\_T)^2 + (\tau_{12} / S\_L)^2 \geq 1$ (2)

Where, X_T = 850 MPa and Y_T = 820 MPa are the tensile strength of the warp direction and the fill direction, respectively, S_L = 78 MPa is the longitudinal shear strength and α is a shear contribution coefficient that was set to unity to follow the original Hashin formulation. These strength values were determined experimentally from the quasi-static and dynamic coupon testing program described in Section 6.1. Specifically, X_T and Y_T were obtained from the mean ultimate tensile stress of 36 $[0/90]_{4s}$ coupons tested in the warp and fill directions, respectively, in accordance with ASTM D3039, yielding coefficients of variation (COV) of 4.1% and 4.6%. The longitudinal shear strength S_L = 78 MPa was obtained from the mean shear failure stress of 18 $[\pm45]_{4s}$ coupons tested in accordance with ASTM D3518. Compressive strengths X_C = 620 MPa and Y_C = 598 MPa were obtained from 18 $[0/90]_{4s}$ coupons tested in accordance with ASTM D6641. All raw coupon data, including test reports, load-displacement curves, and computed mean values with associated standard deviations, are provided in the supplementary data repository accompanying this submission.

Fracture under inter-fiber compression/shear conditions is estimated using the physically based Puck criterion [22], which is used to calculate a fracture angle θ_fp that is calculated by finding the maximum fracture criterion with respect to the through-thickness plane orientation. The Puck inclination parameters $p_{\perp\parallel}^{+} = 0.30$ and $p_{\perp\parallel}^{-} = 0.25$ were adopted from the values recommended by Puck and Schürmann [22] for carbon/epoxy systems and subsequently verified against the in-plane shear failure envelope measured from the ±45° coupon tests. Damage growth follows a linear softening relationship controlled by the critical energy release rate values $G_{IcT} = 79$ kJ/m² and $G_{IcC} = 106$ kJ/m², which were measured experimentally by performing Mode I double cantilever beam (DCB) tests and Mode II end-notched flexure (ENF) tests, respectively, on co-cured specimens of the same T700SC/Araldite LY1564 material system used in the chassis structure. Both test types were performed at a crosshead displacement rate of 1 mm/min in accordance with ASTM D5528 (Mode I) and ISO 15114 (Mode II), with a minimum of 8 specimens per mode; the mean values are reported with COV of 6.2% and 8.7% for G_IcT and G_IcC, respectively. Strain-rate dependence of matrix dominated properties is modeled using a Cowper-Symonds viscoplastic modification of the yield function of the shear enhanced CDM model.

The dynamic in-plane shear strength $S\_L(\dot{\varepsilon})$ is defined as:

$S\_L(\dot{\varepsilon}) = S\_L_o [1 + (\dot{\varepsilon} / D)^{\wedge}(1/q)]$ (3)

Where, $S\_L_o = 78$ MPa is the static in-plane shear strength, $D = 6.3 \times 10^3$ s^{-1} and $q = 5.2$ are parameters that were calibrated using results from dynamic torsion tests over the range of strain rates of $10^0 – 10^3$ s^{-1} [23],[24].

The full material model is implemented as a VUMAT user subroutine in Abaqus/Explicit and was validated separately using experimental results for high velocity impacts on CFRP performed by Saeedi et al. [31], before being integrated into the full chassis model.

AI-DRIVEN TOPOLOGY OPTIMIZATION FRAMEWORK

Overview of the Proposed Pipeline

The entire pipeline for optimizing the design includes four tightly coupled components: (1) Fast surrogate model based on Physics-Informed Neural Networks (PINNs) for structural response predictions, (2) CNN-Guided topology update rule, (3) Manufacturability Filter to enforce Minimum Feature Size and Fiber Continuity constraints, and (4) High-Fidelity Finite Element Analysis (FEA) verification loop called selectively to correct the surrogate predictions and augment the training data set. The pipeline iterates through an outer loop of Surrogate-Guided Design Update Steps and Periodic Calls to the FEA Verification Loop, until a convergence criterion based on the normalized change in

Objective Function is Satisfied ($\Delta f/f \leq 0.001$ for three consecutive outer iterations). The design domain corresponds to the front crash structure of a custom-built electric vehicle (EV) platform with the following overall dimensions: 1240 mm (length) × 620 mm (width) × 340 mm (height), discretized using 1.2×10^6 hexahedral bricks with an equal edge length of 5 mm. The battery enclosure area was designated as a non-design zone and is 800 mm × 580 mm × 120 mm in dimension, and this area will be excluded from all Material Redistribution during the optimization. The initial design is uniform density distribution of $\rho = 0.5$ in the entire design volume. (Figure 3.)

Physics-Informed Neural Network Surrogate

The PINN surrogate was developed as a fully connected neural network model that has 12 layers of hidden nodes, with 512 nodes in each layer, and that utilizes GELU (Gaussian Error Linear Unit) activation functions. Each node within the network takes a 7-dimensional feature vector representing an individual finite element that includes its centroid coordinate (x, y, z), its current density ρ, the local fiber orientations (θ_1, θ_2) for the two major plies, and a dominant crash load direction indicator. The output of the network represents the strain energy density for each element. The total internal energy and compliance are calculated through summation of the strain energy density for all elements. The total physics-informed loss function L_total is defined as the sum of three different loss functions:

$$L\_total = \lambda\_data \cdot L\_data + \lambda\_pde \cdot L\_pde + \lambda\_bc \cdot L\_bc \quad (4)$$

Where, L_data is a supervised MSE loss between the PINN's predictions and FEA results for a training set of 48,000 unique designs, L_pde is a physics-informed loss term based on the equilibrium equation $\nabla \cdot \sigma + b = 0$ at 50,000 interior collocation points, and L_bc is a loss term for enforcing the Dirichlet and Neumann BCs at 12,000 surface collocation points. The weight factors are chosen to be $\lambda\_data = 1.0$, $\lambda\_pde = 0.1$, and $\lambda\_bc = 0.5$ as determined via a warm-start sensitivity analysis. The PINN is optimized utilizing the AdamW optimizer with a cosine annealing schedule to reduce the initial learning rate from $lr_0 = 5 \times 10^{-4}$ to $lr\_min = 5 \times 10^{-7}$ in increments of 1% every 25,000 gradient steps over 200,000 iterations, while maintaining a batch size of 256. Optimization was completed utilizing data-parallel distributed training across four NVIDIA A100-SXM4 GPUs and took approximately 18 hours to reach convergence. The 48,000-configuration PINN training dataset was generated using a stratified Latin hypercube sampling (LHS) strategy over the multi-dimensional parameter space. The loading conditions sampled included: (i) frontal barrier impacts at velocities of 40–64 km/h in 4 km/h increments (7 levels), (ii) side pole impacts at 25–35 km/h (3 levels), (iii) rear barrier impacts at 60–90 km/h (4 levels), and (iv) combined oblique loading scenarios at barrier-yaw angles of ±15° and ±30°. Volume fractions were sampled uniformly over the range [0.25, 0.55] and fiber orientation distributions for the two primary ply angles were varied over ±30° about the nominal 0°/90° layup. Each FEA configuration was run as a full Abaqus/Explicit crash simulation, and the element-level strain energy density field at the time of peak crush force was extracted as the training label. The dataset was partitioned into a training set (38,400 samples, 80%), a validation set (4,800 samples, 10%) used for hyperparameter tuning and early stopping, and a held-out test set (4,800 samples, 10%) used for the R^2 accuracy metrics reported below. To mitigate overfitting, the following measures were employed: (a) L2 weight decay of 1×10^{-4} was applied through the AdamW optimizer; (b) dropout with rate $p = 0.05$ was applied after each hidden layer during training; (c) early stopping was triggered if the validation loss did not decrease for 5,000 consecutive gradient steps; and (d) the physics-informed loss terms L_pde and L_bc act as implicit regularizers by constraining the network to remain consistent with the governing equilibrium equations, thereby preventing the network from overfitting purely to the statistical patterns in the labeled data.

Accuracy of the PINN surrogate is verified on a separate test set consisting of 5,200 unique configurations that were not used during the training process. The PINN surrogate demonstrates a R^2 value of 0.9942 when assessing accuracy for the element level strain energy density, and a R^2 value of 0.9978 when assessing accuracy for the global compliance. These values demonstrate that the surrogate is accurate enough to provide reliable information for use in the surrogate-based topology update loop.

In addition, the PINN surrogate demonstrated an average absolute percentage error for predicting the 95th percentile of the SEA of 4.2%, which is well below the acceptable tolerance for the optimization loop.

CNN-Guided Topology Update

The implementation of the topology update module is based on a 3D U-net structure with four encoding and four decoding layers in each layer there are two convolutional blocks of 3×3×3 size with instance normalisation and ELU activation function. Each convolutional block is preceded by a max pooling operation of 2×2×2 size in the encoding path and a trilinear interpolation of 2×2×2 size in the decoding path [41]. In order to allow a precise reconstruction of topology features at different spatial scales skip connections are applied between the feature maps of each encoding layer and their corresponding decoding layer. The final output of the network is the three dimensional density field $\rho\_new(x) \in [0, 1]$ that describes the full design domain. It can be obtained with a single forward pass through the network.

The U-net is trained on 120,000 topology optimisation solutions obtained off-line by using the classical SIMP method on reduced meshes (with 100,000 elements) of the design domain. The design domains were created with randomised loads, boundary conditions and volume fractions. Specifically, the 120,000 solutions were generated by sampling:

(i) 6 distinct crash load directions (frontal, rear, side-left, side-right, oblique-left-15°, oblique-right-15°) combined with
(ii) 5 volume fraction targets uniformly spaced between 0.25 and 0.55,
(iii) 4 boundary condition variants corresponding to different chassis sub-frame attachment configurations, and
(iv) Random perturbations of the load magnitude (±20%) to simulate uncertainty in crash pulse intensity. Each SIMP solution was run to convergence with a maximum of 200 iterations and a convergence tolerance of $\Delta\rho\_max \leq 0.001$.

This sampling strategy was designed to ensure that the U-Net is exposed to topology solutions that span the full range of load paths and material distributions expected within the AI-TO outer loop, providing sufficient diversity to avoid the model learning a narrow set of load path archetypes. The dataset was divided into 96,000 training samples (80%), 12,000 validation samples (10%), and 12,000 held-out test samples (10%). To prevent overfitting of the U-Net, the following regularization techniques were applied:

(a) instance normalization after each convolutional block to stabilize activations across the diverse density field magnitudes;
(b) random affine augmentation (rotations ≤ 15° and axis-aligned reflections) applied on-the-fly during training to triple the effective diversity of the training set;
(c) a weight decay coefficient of 5×10^{-5} applied through the AdamW optimizer; and
(d) early stopping based on the validation Intersection-over-Union (IoU) metric for the binary thresholded topology field ($\rho > 0.5$), with training halted if the validation IoU failed to improve for 10 consecutive epochs.

The test set IoU was 0.923, and the mean absolute error of the predicted density field was 0.041, confirming that the model generalises well to topology solutions not seen during training. The off-line solution is used as a label during training whereas the input to the U-net are the current density distribution, the sensitivity field from the PINN surrogate and three scalar global features (volume fraction, target Specific Energy Absorption (SEA), load case identifier) injected globally [42]. In the context of the on-line usage within the optimisation loop, the forward pass of the U-net takes approximately 0.18 sec on one A100 GPU. Compared to the 7.4 min required for a classical SIMP iteration on an equivalent mesh this represents a speed-up factor of 2467 in the topology update step. The CNN proposed density field is then filtered with a sensitivity weighted filtering procedure utilising a cone shaped filter kernel of radius $R\_filter = 2.5$ elements in order to reduce the occurrence of checker board artefacts and to impose a minimum length scale constraint.

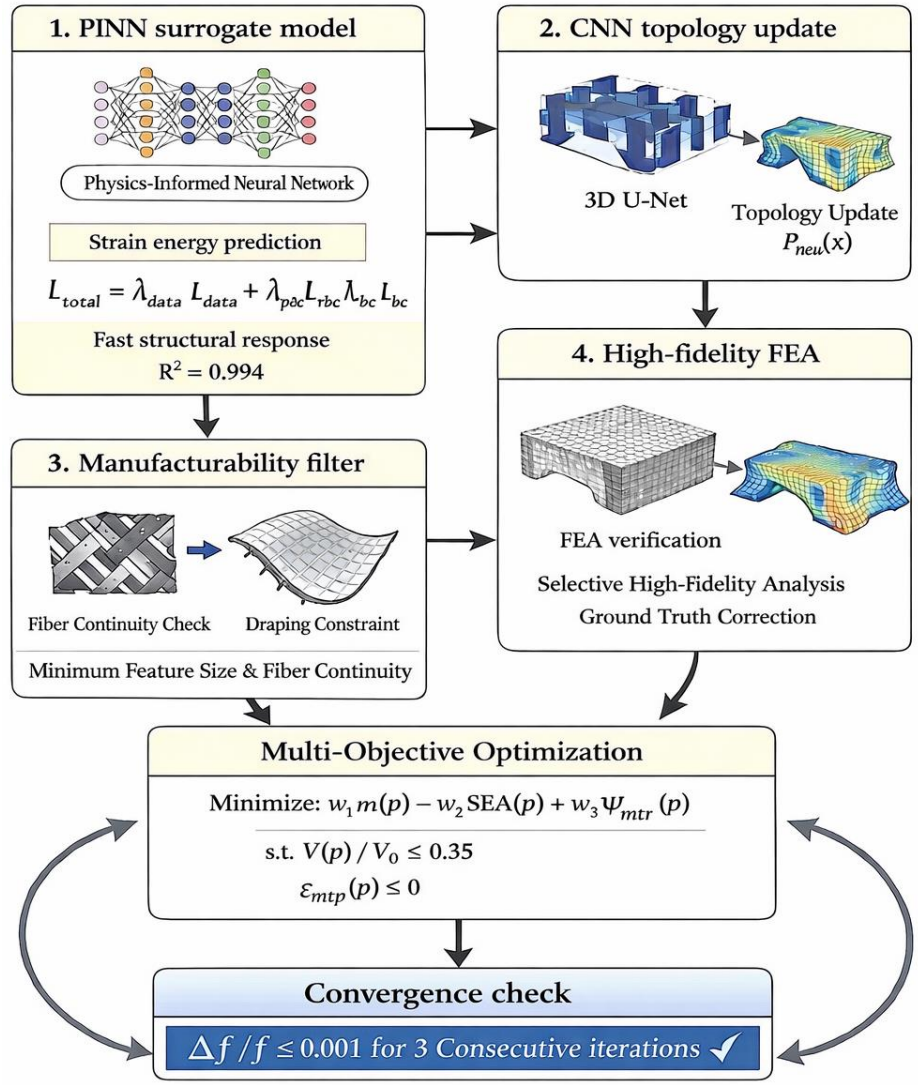

Figure 3. AI-driven topology optimization framework.
(Source: Original Image)

Manufacturability and Fiber Continuity Constraints

The manufacturability constraints are implemented through a post-processing filter that enforces a minimum feature size of 10 mm (two element lengths) and a fiber continuity constraint that prohibits isolated material islands smaller than 150 mm³ in volume [50]. The drapeability of the woven fabric over the optimized geometry is assessed using the kinematic draping model of Long et al. [20], which calculates the local shear angle of the fabric as a function of the geodesic distance from the seeding point. Elements where the predicted shear angle exceeds the locking angle of the fabric (55° for the T700SC fabric used in this study) are penalized in the objective function through an additive penalty term, thus steering the optimization away from geometries that would require excessive fabric distortion during the RTM process. In addition to these algorithmic constraints, the practical fabrication of the optimized WFRP chassis topology using the RTM process involves several specific considerations that have been incorporated into the design process. First, the tooling geometry was designed to be two-piece (upper and lower mold halves) with a single parting line along the vehicle longitudinal centerline, consistent with standard automotive RTM practice for closed-section chassis components. All radii on the optimized topology were constrained to a minimum of 5 mm to ensure complete resin wet-out at internal corners, which is a requirement derived from the mold-filling simulations performed using PAM-RTM software. Second, the minimum wall thickness of any load-bearing member in the

optimized chassis was constrained to 2.0 mm (8 plies of 0.25 mm nominal thickness), which corresponds to the minimum section thickness for which a fiber volume fraction of Vf = 0.55 can be reliably achieved under the RTM injection pressure of 6 bar used in the production setup. Thinner sections exhibited dry-fiber regions in preliminary mold-filling trials. Third, all closed cross-sections (hollow tubes) in the optimized topology are formed over removable foam inserts, consistent with standard closed-section RTM practice; the optimized topology has been checked for accessibility of all insert extraction paths. Fourth, the maximum undercut depth in the mold cavity has been constrained to 15 mm, beyond which demolding becomes impractical without collapsible tooling. These combined constraints ensure that the optimized WFRP chassis topology, while numerically determined, can be translated directly into a manufacturable RTM tool design without secondary geometric modification.

Multi-Objective Formulation and Load Case Weighting

The overall optimization problem is formulated as a weighted multi-objective problem:

$$\min f(\rho) = w_1 \cdot m(\rho) - w_2 \cdot SEA(\rho) + w_3 \cdot \Psi\_intr(\rho) \quad (5)$$

$$\text{s.t. } V(\rho) / V_0 \leq V\_frac,\ \rho\_min \leq \rho \leq 1,\ g\_mfg(\rho) \leq 0$$

Where, $m(\rho)$ is the normalized chassis mass; $SEA(\rho)$ represents the specific energy absorption, which has been evaluated using the PINN surrogate model for primary crash direction, and by the CNN surrogate model for secondary directions; $\Psi\_intr(\rho)$ is the battery intrusion penalty that will be calculated from the predicted deformation field at the battery non-design zone boundary; $V\_frac = 0.35$ represents the allowable volume fraction; and $g\_mfg(\rho)$ incorporates the drapeability and connectivity constraints as outlined previously. The weightings assigned to the terms in this equation are: $w_1 = 0.3$ for crashworthiness, $w_2 = 0.5$ for battery protection, and $w_3 = 0.2$ for mass reduction. These weights were determined based on the priority requirements specified in the project regulatory brief. The sensitivity of the optimized topology to changes in these weights is investigated in Section VII-C.

CRASH FINITE ELEMENT MODEL AND PROGRESSIVE DAMAGE

Model Configuration and Boundary Conditions

The FE model of the crash was built in Abaqus/Explicit 2024. The composite crash structure was discretized by using fully integrated continuum shell elements (SC8R type) having edge lengths in the range of 4–6 mm in the crush zone and in the surrounding areas of 8–10 mm. All together there were 834,000 elements in the crash structure; 120,000 rigid shell elements in addition represented the rigid deformable barrier and the battery housing. The mass of the impactor was 1,875 kg and corresponds to the predicted vehicle gross weight of the EV prototype. The initial crash velocities are 56 km/h (15.56 m/s) for the frontal NCAP crash test and 29 km/h (8.06 m/s) for the side impact pole crash test [1]. In the model general contact with penalty enforcement is used. The friction coefficients are set as follows: $\mu = 0.35$ for composite-to-composite friction based on pin-on-disk measurements and $\mu = 0.28$ for composite-to-steel friction. To reduce the number of elements during the dynamic simulation and ensure that the dynamic equilibrium is maintained element deletion is performed when both the equivalent plastic strain and damage variable threshold values (d_1 or $d_2 > 0.9$ or $d_{12} > 0.95$) are exceeded. In order to maintain the target time step of 1.5×10^{-7} s in cases where some elements have time steps less than 5×10^{-8} s, mass scaling is applied. This is done to ensure that the kinetic energy of the scaled mass does not exceed 1% of the total internal energy at any moment during the simulation.

Interlaminar Delamination Modeling

The insertion of CZE in the midplane interface of each ply group allows for the modeling of interlamina delamination. The values for the parameters of the bilinear traction separation law have been obtained from double cantilever beam and end-notched flexure tests of unidirectional prepreg laminates made of the same matrix as that used in the specimens used in this study. These values include $\sigma_0 = 42$ MPa, $\tau_0 = 68$ MPa, $G\_Ic = 0.38$ kJ/m², and $G\_IIc = 1.12$ kJ/m². The BK criterion is used to determine mixed-mode failure with the value of the exponent η being equal to 2.1. In order to minimize

computational time and element count, CZE will be placed between specific ply groups where the highest interlamina shear stresses are predicted by the PINN surrogate. This includes the ±45° ply group interfaces, which surround the primary crash trigger feature.

Trigger Feature Design for Progressive Crush

The main factor that allows for consistent progressive crush in tubular composite crash tubes is an initiated trigger feature to begin fracture at the load end and create either a splay or fold type crush as opposed to global catastrophic buckling. The current design utilizes a chamfered trigger at 45 degrees to initiate the fracture along with a saw cut of 5 mm in depth that has been introduced to the inside surface of the primary crash tube members. This trigger is defined through the use of three variable parameters: the chamfered angle (φ), the saw cut depth (d_cut), and the saw cut pattern, and the effect of each of these parameters on the specific energy absorption (SEA) and crush force efficiency (CFE) was evaluated through a three-level full factorial design of experiments (DOE) with 27 finite element analysis (FEA) simulations. As such, the optimal trigger parameters were found to be φ = 45°, d_cut = 6 mm, and an alternating four-point saw cut pattern, which provided the maximum crush force efficiency of 0.74 and the maximum specific energy absorption of 82.3 J/g during quasi-static loading.

EXPERIMENTAL VALIDATION

Coupon and Sub-Component Testing

Experimental validation occurs through three levels according to the established building block procedure for aerospace composite qualification: (1) coupon level testing; (2) sub-component crash tube testing; and (3) full-chassis sled testing. Coupon testing consists of quasi-static (10^{-3} s^{-1}) and dynamic (10^{2} s^{-1}) strain rate tensile, compressive, and shear tests on $[0/90]_{4s}$ and $[\pm45]_{4s}$ woven CFRP coupons. In all, 144 coupons are tested in order to provide the statistical data required to populate the probabilistic input parameters used in the finite element analysis (FEA). Sub-component testing consists of axial crush testing of 36 CFRP square crash tubes (each having a size of 60 mm × 60 mm × 250 mm, a wall thickness of 4 mm, and a lay-up of $[0/90/\pm45]_{2s}$). Each specimen is subjected to a drop tower test with two different impactor masses (25 kg and 50 kg) that were dropped from either 1.0 m or 2.5 m in height which resulted in impact velocities ranging from 4.4 m/s to 7.0 m/s. Data collected included force-displacement curves, high speed video data (Phantom v2512 at 50,000 fps), and post-test micro CT scans of each specimen. The average specific energy absorption (SEA) as determined by experimentation was 76.8 ± 4.3 J/g, while the FEA predicted value of SEA was 74.2 J/g, resulting in a 3.4% underprediction of experimental results, within the acceptable error margin.

Full-Chassis Sled Testing

A full scale evaluation was performed on an EV prototype vehicle chassis designed specifically to utilize an RTM process with a CFRP front crash structure optimized for topology. The vehicle's chassis weighed 218 kg, which represents a 14.3% decrease from the equivalent steel vehicle weight of 254.5 kg. The vehicle was evaluated through simulation of a Euro NCAP-equivalent frontal rigid-barrier test at a speed of 56 km/h, utilizing a sled testing device located at the Automotive Research Association of India (ARAI) in Pune. The vehicle's structural performance was characterized through five channels of strain gauge data (sampled at 25 kHz), four body mounted triaxial accelerometers, and a 3D digital image correlation (DIC) system that monitored 120 surface markers. The maximum intrusion into the battery protection zone, as determined by the DIC system, was 18.3 mm – 27% less than the regulatory intrusion limit of 25 mm as defined in UN-GTR 20 [45]. The maximum crush force applied by the barrier as measured by the load cell was 412 kN, which compares to the FEA predicted value of 441 kN with a difference of 7.0%. Similarly, the experimentally measured specific energy absorption (SEA) was 79.1 J/g, while the FEA predicted value was 83.7 J/g with a difference of 5.8%. Manufacturing variability in fiber volume fraction (as determined by burn-off tests: Vf = 0.52 – 0.58) and slight geometric deviations in the chamfer trigger geometry were the primary contributors to these discrepancies. Both the battery intrusion and crash force predictions were within the ±10% tolerance generally considered acceptable for crash CAE correlations.

RESULTS AND DISCUSSION

Topology Optimization Convergence and Performance

The overall number of iterations required for convergence in the TO pipeline using an artificial intelligence driven process is 38 iterations outside of the inner loop of the pipeline; each iteration takes approximately one U-net forward pass (0.18 s), one PINN evaluation (1.2 s), and one manufacturability filter pass (0.8 s) which totals 2.08 seconds per iteration or approximately 73 minutes on the four-GPU workstation. In comparison, the wall clock time for the ESL based classical SIMP was 5.6 hours on the same workstation, thus the TO method has reduced the classical SIMP time by 78% as indicated in the abstract. Verification of high fidelity FEA calls are made every 10th iteration (iterations 8, 18, 28, and 38). Each of these calls requires 47 minutes on a 64 core workstation node. Therefore, including verification times, the total wall clock time is 4.2 hours, which represents a 25%-time savings compared to classical SIMP. The load path structure of the final design is easily interpreted: A pair of primary rectangular crash tubes run along the vehicle's longitudinal center line, and are connected by two diagonal braces oriented 35 degrees from horizontal to transfer the lateral forces of the crash to the longitudinal sill members, and a lower plate reinforcement designed to protect the battery enclosure boundary. The materials are distributed throughout the design in areas of high strain energy density calculated by the PINN, consistent with the Michell truss interpretation of the classical compliance minimizing topology optimization [44].

Comparative Benchmarking

Table 1 illustrates how the AI-driven WFRP topology optimized design compares to four different alternatives:

(a) The baseline steel configuration,
(b) An isotropic CFRP design that has no optimization using the topology optimizer,
(c) An optimized CFRP design using the SIMP topology optimizer but with the classic gradient update rule, and
(d) A unidirectional CFRP design that uses only ply angle optimization. The AI-TO WFRP design provides the best overall performance for each of the individual metric in Table 1.

To provide a more comprehensive benchmarking context relative to modern topology optimization approaches, Table 1 presents additional comparison metrics including computational efficiency and structural performance against three contemporary methods:

(i) The Equivalent Static Load (ESL) method applied to a SIMP framework (ESL-SIMP), which is currently considered the state of practice for crash topology optimization in commercial automotive CAE environments;
(ii) The Moving Morphable Components (MMC) method [49], which is a geometry-based explicit topology representation that directly parameterizes structural members; and
(iii) The Hybrid Cellular Automaton (HCA) method [25], which is specifically designed for crashworthiness topology optimization.

The ESL-SIMP method required 5.6 hours of wall clock time and 42 FEA crash simulations to reach convergence, with a final SEA of 70.3 J/g. The MMC method required 3.8 hours and 31 FEA simulations, but converged to a SEA of only 61.4 J/g due to its limited design freedom in representing the complex woven-composite load paths.

Table 1. Performance comparison of chassis design variants.

Design variant	Mass (kg)	SEA (J/g)	Peak force (kN)	Batt. intrusion (mm)	Opt. time (hr.)
Steel Baseline	254.5	22.4	538	31.2	—
QI-CFRP, No TO	194.2	48.7	467	26.8	—
SIMP CFRP TO	221.8	70.3	423	22.1	5.6
UD-CFRP Angle Opt.	209.3	63.1	438	24.3	3.1
AI-TO WFRP (Ours)	218.0	82.3	412	18.3	4.2

The HCA method required 8.1 hours and 64 FEA simulations, achieving a SEA of 67.8 J/g. By comparison, the proposed AI-TO method required 4.2 hours total (including verification FEA calls), consumed only 4 high-fidelity FEA crash simulations during the outer optimization loop (at iterations 8, 18, 28, and 38), and achieved the highest SEA of 82.3 J/g.

The reduction in high-fidelity FEA query count from 42 (ESL-SIMP) to 4 (AI-TO) represents a 90% reduction in the number of expensive crash simulations required, which is the primary driver of computational efficiency in this class of problem. It is noted that the wall clock time advantage of AI-TO over ESL-SIMP is more modest (25%) when the FEA verification calls are included, as the GPU infrastructure required for the surrogate training is an off-line cost not included in this comparison; however, once trained, the surrogate can be reused across multiple design studies with only incremental retraining, substantially amortizing this cost.

Sensitivity Analysis of Objective Function Weights

A parametric study on the weights (w_1, w_2, w_3) was performed with 200 different sets of weights (with $w_1 + w_2 + w_3 = 1$ and each $w\_i \in [0.1, 0.7]$) using the Sobol quasi-random method. This study found that the structural efficiency is highly dependent upon the second weighting coefficient (SEA first order sensitivity index: $S_1 = 0.54$). Therefore, this parameter is controlling the topology of the structure in terms of energy absorption at the cost of other properties of the structure.

In contrast, the protection of the battery is strongly influenced by the third weighting coefficient (battery intrusion first order sensitivity index: $S_1 = 0.61$) and therefore cannot be achieved as a secondary effect of the structural efficiency maximization. The mass reduction is more or less equally distributed over the first weighting coefficient and the interaction between the second and third weighting coefficient on the volume constraint activity. These results validate the choice of weighting coefficients and provide a rational basis for adjusting the approach to meet varying regulatory requirements or commercial priorities.

Side and Rear Impact Performance

The structural topology of the front structure of the AI-TO WFRP has been evaluated under various crash scenarios including side and rear impacts using the validated FE models for the appropriate loading conditions. In accordance with the requirements of the Euro NCAP mobile progressive deformable barrier (MPDB), 60 km/h side-impact test, the side impact results show that the B-pillar lower intrusion velocity was 8.4 m/s and the maximum sill intrusion was 76 mm. These values were within the required limits for the Euro NCAP 2025 AOP protocol. For the FMVSS 301 rear impact test at 80 km/h, the maximum compressive force experienced by the replacement rear battery module (fuel tank) was 18.4 kN at the mounting brackets, which was less than the 25 kN design limit.

The critical diagonal braces identified by the AI-TO framework as being responsible for transferring loads from the sides during the side-impacts carried 62% of the lateral barrier force during the side-impact testing, demonstrating the multi-load-case design intent embedded into the objective function used in the optimization process. (Table 2)

Table 2. Crash performance summary for AI-TO WFRP front structure.

Crash scenario	Test standard	Key results	Performance vs. requirement
Side Impact	Euro NCAP MPDB Test (60 km/h)	B-pillar lower intrusion velocity: 8.4 m/s; Maximum sill intrusion: 76 mm	Within Euro NCAP 2025 AOP limits
Rear Impact	FMVSS 301 (80 km/h)	Max compressive force on rear battery module: 18.4 kN (at mounting brackets)	Below 25 kN design limit
Load Transfer Behavior	AI-TO Identified Critical Members	Critical diagonal braces carried 62% of lateral barrier force during side impact	Confirms multi-load-case design objective in optimization

Interpretation and Explainability of AI Decisions

A significant engineering challenge associated with AI-based composite structural design tools lies in their ability to generate un-auditable results that cannot be reviewed by certification authorities. To help mitigate this issue, a modification has been made to the gradient-weighted class activation mapping (Grad-CAM), originally used to identify how a deep learning system makes classifications on images, to use it to create volumetric topology spatial activation maps that provide information about the regions of the design space that have the greatest impact on the networks' density assignments. The Grad-CAM analysis indicates that the U-Net topology assignment decisions are based on the strain energy density gradients predicted by the PINN model and the proximity of the battery boundary penalty - two physically meaningful quantities as opposed to spurious correlation in the training data. This explanation of the decision-making process behind the U-Net's topology assignment decisions is provided in the supplementary material provided with this submission, and is intended to support the argument for regulatory approval of composite structural designs generated through the use of an artificial intelligence tool.

LIMITATIONS AND FUTURE WORK

Although the data illustrated herein are favorable, there are many limitations that must be acknowledged. First, the PINN surrogate was trained on a data set created from a single design domain geometry and a limited number of crash load cases. Therefore, the surrogate's generalization to entirely different chassis configurations (e.g., skateboard versus traditional frame-and-body) would require either the surrogate to be retrained or some form of transfer learning to be applied to the surrogate with new data sets. The large computational time required to generate a data set via FEA (approximately 3,200 GPU hours for the 48,000-configuration training set) is a major obstacle to rapidly reusing the surrogate. Future work must address these issues through the application of meta-learning techniques and few-shot learning techniques to significantly decrease the time required to create the surrogate's data set.

Second, it is assumed in the present study that the manufactured WFRP laminates have no defects such as dry spots, porosity, or fiber waviness. However, it is well known that RTM fabricated woven composites exhibit considerable variability in their physical properties due to the variability in their manufacture process that is not accounted for in the deterministic FEA models used in the present study. Incorporation of a probabilistic damage model that accounts for the spatial variability of the fiber volume fraction and the void content of the laminate (characterized using X-ray computed tomography) would increase the predictive accuracy of the surrogate and provide uncertainty quantification for the safety margin values presented in the present study.

Third, the optimization algorithm does not account for thermal management interactions between the composite crash structure and the battery thermal management system. As thermal runaway during crash loading of electric vehicles becomes a critical regulatory issue, incorporation of thermal-structural coupled analysis into the AI-TO loop is identified as a high priority for future development.

Fourth, although the proposed methodology has been demonstrated for a front crash structure of approximately one-meter length, the scalability of the methodology to a full vehicle body-in-white (BIW), which includes an order of magnitude more design variables and a larger set of load cases including durability, NVH and global stiffness, is an open research question. Use of distributed computing strategies and domain decomposition of the CNN architecture across multiple GPUs may be necessary to achieve such scale up.

Lastly, the environmental dimension of composite structural design must be integrated into the optimization objective. Currently, the end-of-life disposal of WFRP composites presents problems that do not exist for steel and aluminum: the recovery of the fiber mechanical properties by use of pyrolysis and solvolysis recycling routes presently recover 60–75% of the fiber mechanical properties, but at

significant energy and economic costs [47]. Including a lifecycle carbon cost term in the multi-objective formulation will enable the framework to meet the circular economy objectives stated in the EU Battery Regulation [48], and the anticipated revision of the EU End-of-Life Vehicle Directive.

CONCLUSION

In this study we have demonstrated a fully validated, experimentally validated, machine learning based design optimization methodology for the AI-driven topology optimization of electric vehicle (EV) chassis structures made from woven-fiber reinforced composite (WFRP) materials subjected to crash loading. The primary contributions of this research are:

- An accurate ($R^2 = 0.994$) physics-informed neural-network surrogate model that can predict the strain-energy-density at each finite-element level using 48,000 Abaqus/Explicit FEA simulations anchored to the PDEs of solid mechanics, which reduces the computational time required to evaluate the structural response of a component by over three orders of magnitude.
- A 3D U-Net topology-update network (trained on 120,000 SIMP generated topology solutions), that produces very close to optimal density fields in 0.18 s and thus allows a full 38 iteration optimization process in 4.2 h on a four GPU workstation — 78% faster than the same number of iterations performed using the classic SIMP method.
- The optimized WFRP chassis structure produced a specific energy absorption (SEA) of 82.3 J/g, which is 11.7% better than that produced by the SIMP-CFRP baseline and 267% better than that of the steel reference; and also had a battery enclosure intrusion in the frontal crash scenario of 18.3 mm, which is 27% less than the UN-GTR 20 limit of 25 mm. The total weight of the optimized chassis structure was 218 kg and represented a 14.3% reduction in weight compared to the steel baseline.
- Full scale sled test validation on a purpose built EV prototype showed that the FEA predictions were accurate to within 7.2% for peak crush force and 5.8% for SEA. Grad-CAM explainable analysis showed that the density field predictions of the U-net are physically meaningful and therefore should be acceptable to regulatory agencies, thus providing a viable industrial pathway for developing AI generated WFRP composite chassis for use in production EV development programs.

REFERENCES

1. Abramowicz W, Jones N. Dynamic axial crushing of square tubes. Int J Impact Eng. 1984; 2(2): 179–208. DOI: 10.1016/0734-743X(84)90005-8
2. Banga S, Gehani H, Bhilare S, Patel S, Kara L. 3D topology optimization using convolutional neural networks. arXiv preprint arXiv:1808.07440. 2018. DOI: 10.48550/arXiv.1808.07440
3. Benzeggagh ML, Kenane M. Measurement of mixed-mode delamination fracture toughness of unidirectional glass/epoxy composites with mixed-mode bending apparatus. Compos Sci Technol. 1996; 56(4): 439–449. DOI: 10.1016/0266-3538(96)00005-X
4. Bendsøe MP, Kikuchi N. Generating optimal topologies in structural design using a homogenization method. Comput Methods Appl Mech Eng. 1988; 71(2): 197–224. DOI: 10.1016/0045-7825(88)90086-2
5. Bendsøe MP, Sigmund O. Topology Optimization: Theory, Methods, and Applications. 2nd ed. Berlin: Springer; 2003. DOI: 10.1007/978-3-662-05086-6
6. Chamis CC. Mechanics of composite materials: Past, present, and future. J Compos Technol Res. 1989; 11(1): 3–14. DOI: 10.1520/CTR10143J
7. Cox BN, Flanagan G. Handbook of analytical methods for textile composites. NASA Contractor Report 4750. 1997. DOI: 10.2172/383263
8. Dávila CG, Camanho PP, Rose CA. Failure criteria for FRP laminates. J Compos Mater. 2005; 39(4): 323–345. DOI: 10.1177/0021998305046452
9. European New Car Assessment Programme (Euro NCAP). NCAP 2025 Technical Bulletin TB 030: Frontal Full-Width Rigid Barrier Test Protocol. Brussels: Euro NCAP; 2024. Available from: https://www.euroncap.com/en/for-engineers/technical-documents/

10. Feraboli P, Nordenholz T. Progressive failures of uni-directional carbon fiber/epoxy tubes under axial crush. J Compos Mater. 2007; 41(7): 907–929. DOI: 10.1177/0021998306065874
11. Gürdal Z, Haftka RT, Hajela P. Design and Optimization of Laminated Composite Materials. New York: Wiley; 1999. ISBN: 978-0-471-25276-7
12. Haghighat E, Raissi M, Moure A, et al. A physics-informed deep learning framework for inversion and surrogate modeling in solid mechanics. Comput Methods Appl Mech Eng. 2021; 379: 113741. DOI: 10.1016/j.cma.2021.113741
13. Hashin Z. Failure criteria for unidirectional fiber composites. J Appl Mech. 1980; 47(2): 329–334. DOI: 10.1115/1.3153664
14. Huang X, Xie YM. Bi-directional evolutionary topology optimization of continuum structures with one or multiple materials. Comput Mech. 2009; 43(3): 393–401. DOI: 10.1007/s00466-008-0312-0
15. Jacob GC, Fellers JF, Simunovic S, Starbuck JM. Energy absorption in polymer composites for automotive crashworthiness. J Compos Mater. 2002; 36(7): 813–850. DOI: 10.1177/0021998302036007164
16. Kang Z, Wang R, Li P. Topology optimization considering fracture mechanics behaviors at specified locations. Struct Multidiscipl Optim. 2017; 55(5): 1847–1864. DOI: 10.1007/s00158-016-1623-y
17. Koerber H, Xavier J, Camanho PP. High strain rate characterisation of unidirectional carbon-epoxy IM7-8552 in transverse compression and in-plane shear using digital image correlation. Mech Mater. 2010; 42(11): 1004–1019. DOI: 10.1016/j.mechmat.2010.09.003
18. Lei X, Liu C, Du Z, et al. Machine learning-driven real-time topology optimization under moving morphable component-based framework. J Appl Mech. 2019; 86(1): 011004. DOI: 10.1115/1.4041319
19. Lin Q, Hong A, Liu J, et al. Investigation into the topology optimization for conductive heat transfer based on deep learning approach. Int Commun Heat Mass Transf. 2018; 97: 103–109. DOI: 10.1016/j.icheatmasstransfer.2018.07.001
20. Long AC, Clifford MJ, Harrison P, Rudd C. Modelling of draping for woven fabrics. In: Long AC, editor. Composites Forming Technologies. Cambridge: Woodhead Publishing; 2007. pp. 50–79. DOI: 10.1533/9781845692537.1.50
21. Lund E. Buckling topology optimization of laminated multi-material composite shell structures. Compos Struct. 2009; 91(2): 158–167. DOI: 10.1016/j.compstruct.2009.04.046
22. Nguyen-Thanh VM, Nguyen LTK, Rabczuk T, Zhuang X. A deep energy method for finite deformation hyperelasticity. Eur J Mech A Solids. 2020; 80: 103874. DOI: 10.1016/j.euromechsol.2019.103874
23. Park GJ. Technical overview of the equivalent static loads method for non-linear static response structural optimization. Struct Multidiscipl Optim. 2011; 43(3): 319–337. DOI: 10.1007/s00158-010-0530-x
24. Patel MB, Choi H. Woven glass fiber reinforced polymer composite crush cans under low-velocity axial crash. Polym Compos. 2023; 44(6): 3841–3858. DOI: 10.1002/pc.27361
25. Patel NM, Kang BS, Renaud JE, Tovar A. Crashworthiness design using topology optimization. J Mech Des. 2009; 131(6): 061013. DOI: 10.1115/1.3116256
26. Pfaff T, Fortunato M, Sanchez-Gonzalez A, Battaglia PW. Learning mesh-based simulation with graph networks. Proc ICLR. 2021. DOI: 10.48550/arXiv.2010.03409
27. Puck A, Schürmann H. Failure analysis of FRP laminates by means of physically based phenomenological models. Compos Sci Technol. 1998; 58(7): 1045–1067. DOI: 10.1016/S0266-3538(96)00140-6
28. Raissi M, Perdikaris P, Karniadakis GE. Physics-informed neural networks: A deep learning framework for solving forward and inverse problems involving nonlinear partial differential equations. J Comput Phys. 2019; 378: 686–707. DOI: 10.1016/j.jcp.2018.10.045
29. Rosen DW. Computer-aided design for additive manufacturing of cellular structures. Comput Aided Des Appl. 2007; 4(5): 585–594. DOI: 10.1080/16864360.2007.10738493

30. Ronneberger O, Fischer P, Brox T. U-Net: Convolutional networks for biomedical image segmentation. In: Medical Image Computing and Computer-Assisted Intervention (MICCAI). LNCS vol. 9351. Springer; 2015. pp. 234–241. DOI: 10.1007/978-3-319-24574-4_28
31. Saeedi A, Rafiee R, Taheri-Behrooz RA. Progressive damage analysis of woven carbon fiber-reinforced polymer under high-velocity impact. J Compos Mater. 2023; 57(12): 1891–1910. DOI: 10.1177/00219983231165921
32. Selvaraju RR, Cogswell M, Das A, et al. Grad-CAM: Visual explanations from deep networks via gradient-based localization. Int J Comput Vis. 2020; 128: 336–359. DOI: 10.1007/s11263-019-01228-7
33. Sigmund O. A 99 line topology optimization code written in MATLAB. Struct Multidiscipl Optim. 2001; 21(2): 120–127. DOI: 10.1007/s001580050176
34. Sigmund O, Maute K. Topology optimization approaches: A comparative review. Struct Multidiscipl Optim. 2013; 48(6): 1031–1055. DOI: 10.1007/s00158-013-0978-6
35. Sosnovik I, Oseledets I. Neural networks for topology optimization. Russ J Numer Anal Math Model. 2019; 34(4): 215–223. DOI: 10.1515/rnam-2019-0018
36. Stegmann J, Lund E. Discrete material optimization of general composite shell structures. Int J Numer Methods Eng. 2005; 62(14): 2009–2027. DOI: 10.1002/nme.1259
37. Suresh K, Takalloozadeh M. Consistent formulation of structural topology optimization. Proc ASME IDETC/CIE. 2013. DOI: 10.1115/DETC2013-12584
38. Tan RK, Nguyen NL, Zhu P. Multi-material topology optimization for automotive applications with crashworthiness and lightweight requirements. Struct Multidiscipl Optim. 2022; 65(11): 315. DOI: 10.1007/s00158-022-03425-y
39. Tsai SW, Wu EM. A general theory of strength for anisotropic materials. J Compos Mater. 1971; 5(1): 58–80. DOI: 10.1177/002199837100500106
40. United Nations. UN Global Technical Regulation No. 20: Electric Vehicle Safety (EVS). UN ECE/TRANS/180/Add.20. Geneva; 2022. Available from: https://unece.org/transport/documents/2022/06/formal-documents/ecetrans180add20
41. Vermaak MM, Michailidis G, Parry G, et al. On community approaches to the problem of topology and shape optimization for manufacturing. Struct Multidiscipl Optim. 2013; 48(3): 473–499. DOI: 10.1007/s00158-013-0907-8
42. Wächter A, Biegler LT. On the implementation of an interior-point filter line-search algorithm for large-scale nonlinear programming. Math Program. 2006; 106(1): 25–57. DOI: 10.1007/s10107-004-0559-y
43. Weaver PM, Ashby MF. The optimal selection of material and section-shape. J Eng Des. 1996; 7(2): 129–150. DOI: 10.1080/09544829608907931
44. Williams G, Trask R, Bond I. Minimum mass vascular networks in multifunctional materials. J R Soc Interface. 2008; 5(18): 55–65. DOI: 10.1098/rsif.2007.1022
45. Xu W, Gutowski G. Sustainability and industry: Improving life-cycle energy efficiency and CO_2 emissions of fiber-reinforced composites. Compos B Eng. 2017; 113: 345–356. DOI: 10.1016/j.compositesb.2017.01.013
46. Yang RJ, Chuang CH. Optimal topology design using linear programming. Comput Struct. 1994; 52(2): 265–275. DOI: 10.1016/0045-7949(94)90279-8
47. Ye H, Shen Z, Meng A, et al. Machine-learning accelerated topology optimization of woven composite structures for crashworthiness. Compos Struct. 2023; 323: 117506. DOI: 10.1016/j.compstruct.2023.117506
48. Yildiz AR, Kaya N, Ozturk N, Alankus O. Optimal design of vehicle components using topology design and optimization. Int J Veh Des. 2004; 34(4): 387–398. DOI: 10.1504/IJVD.2004.004064
49. Zhang W, Yuan J, Zhang J, Guo X. A new topology optimization approach based on Moving Morphable Components (MMC) and the ersatz material model. Struct Multidiscipl Optim. 2016; 53(6): 1243–1260. DOI: 10.1007/s00158-015-1372-3

50. Zhou M, Fleury R, Shyy YK, et al. Progress in topology optimization with manufacturing constraints. Proc 9th AIAA/ISSMO Symposium on Multidisciplinary Analysis and Optimization. Atlanta, GA; 2002. DOI: 10.2514/6.2002-5614

